Research Article

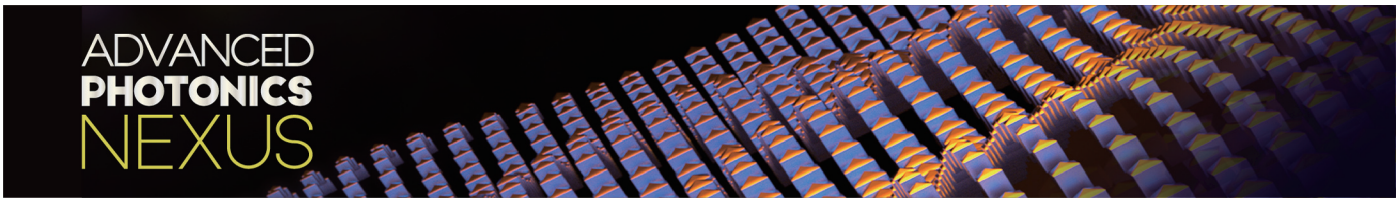

Robust spectral reconstruction algorithm enables quantum dot spectrometers with subnanometer spectral accuracy

Wenkai Ma,[a,†] Qian Xue,[a,†] Yang Yang,[a] Hanqiu Zhang,[a] Daoli Zhang,[a] Xinzheng Lan,[b] Liang Gao,[c,d,e,f] Jianbing Zhang,[a,c,d,f,*] and Jiang Tang[b,c,e]

[a]Huazhong University of Science and Technology, School of Integrated Circuits, Wuhan, China
[b]Huazhong University of Science and Technology, School of Optical and Electronic Information, Wuhan, China
[c]Huazhong University of Science and Technology, Wuhan National Laboratory for Optoelectronics, Wuhan, China
[d]Huazhong University of Science and Technology, Wenzhou Advanced Manufacturing Technology Research Institute, Wenzhou, China
[e]Optics Valley Laboratory, Wuhan, China
[f]Research Institute of Huazhong University of Science and Technology in Shenzhen, Shenzhen, China

Abstract. Since the concept of computational spectroscopy was introduced, numerous computational spectrometers have emerged. While most of the work focuses on materials, optical structures, and devices, little attention is paid to the reconstruction algorithm, thus resulting in a common issue: the effectiveness of spectral reconstruction is limited under high-level noise originating from the data acquisition process. Here, we fabricate a computational spectrometer based on a quantum dot (QD) filter array and propose what we believe is a novel algorithm, TKVA (algorithm with Tikhonov and total variation regularization, and the alternating direction method of multipliers), to suppress the impact of noise on spectral recovery. Surprisingly, the new TKVA algorithm gives rise to another advantage, i.e., the spectral accuracy can be enhanced through interpolation of the precalibration data, providing a convenient solution for performance improvement. In addition, the accuracy of spectral recovery is also enhanced via the interpolation, highlighting its superiority in spectral reconstruction. As a result, the QD spectrometer using the TKVA algorithm shows supreme spectral recovery accuracy compared to the traditional algorithms for complex and broad spectra, a spectral accuracy as low as 0.1 nm, and a spectral resolution of 2 nm in the range of 400 to 800 nm. The new reconstruction algorithm can be applied in various computational spectrometers, facilitating the development of this kind of equipment.

Keywords: microspectrometer; quantum dots; regularization; compressive sensing.

Received Feb. 21, 2024; revised manuscript received May 15, 2024; accepted for publication Jun. 3, 2024; published online Jun. 27, 2024.

[DOI: 10.1117/1.APN.3.4.046009]

1 Introduction

Spectral analysis plays a crucial role in scientific research and industrial production.[1–3] Mainstream spectral analysis is based on spectrometers whose size must be reduced for portable applications and assembling in other systems. Traditional spectrometers face significant challenges in miniaturization and portability due to their complex optical paths and reliance on precision dispersion elements.[4] In recent years, with the continuous advancement of computer technology and optical manufacturing, computational spectrometers have emerged as a promising solution to overcome these challenges.[5]

The uniqueness of computational spectrometers lies in their utilization of various encoding techniques to acquire spectral data, followed by algorithmic reconstruction, and avoiding the dependence on long optical paths and complex optical components. The performance of computational spectrometers is

*Address all correspondence to Jianbing Zhang, jbzhang@hust.edu.cn
†Wenkai Ma and Qian Xue contributed equally to this work.

highly dependent on the specificity of the spectral encoding method and the robustness of the reconstruction algorithm.[6–10] In terms of spectral encoding, a variety of techniques, such as filter arrays,[11–13] detector arrays,[14,15] tunable filters,[16,17] and detectors[18,19] have been proposed. Among these techniques, the quantum dot (QD) filter array is a promising route for computational spectrometers due to the finely tunable absorption spectrum via size and composition and ease of solution processability.[20–22] While most of the study on computational spectrometers has been focused on spectral encoding, there have also been some works dedicated to exploring reconstruction algorithms with higher noise immunity. As a result, a limited number of algorithms, such as least squares regression,[23] Ridge regression,[16] and Lasso regression,[24] have been adopted. Furthermore, the robustness of these algorithms needs to be improved. Noise might emerge during the data acquisition process due to variations of transmittance in the filter array, spectral response in the detector array, or repeatability of tunable filters/detectors. The noise affects the accuracy of spectral reconstruction, imposing a higher requirement on the robustness of the algorithms.[25] The noise tolerance of the aforementioned algorithms still needs improvement. For instance, ordinary least squares regression has minimal noise tolerance, and Lasso regression and Ridge regression also exhibit sensitivity to noise perturbations.[26] In response, new algorithms have been proposed to enhance noise tolerance. For example, an ALM algorithm obtained by combining total variation (TV) regularization with the augmented Lagrange multiplier method improves the noise immunity of the algorithm to some extent, while reconstruction performance decreases under a high noise level.[26] Recently, machine learning was also applied to pursue better robustness of algorithms.[27] Through processing the detected signals using a pretrained denoising autoencoder network before employing the reconstruction algorithm, the noise immunity of the spectrometer system is substantially improved. However, such an algorithm was designed uniquely for its encoding structure and therefore cannot be directly used quickly and inexpensively for other computational spectrometers, but rather again requires the entire process from database creation to model tuning and training. Therefore, it is highly desirable to develop a robust algorithm with a high level of noise tolerance and good migratory properties.

Against this backdrop, this study aims to enhance the tolerance of computational reconstruction spectrometers to noise, thereby further improving their performance. We fabricated a spectrometer based on a QD filter array and proposed a new algorithm with supreme noise tolerance performance. Benefiting from the robust algorithm, the QD spectrometer is capable of accurately reconstructing spectral features even at signal to noise ratio $(\mathrm{SNR}) = -3$ dB, which is remarkably better than the results based on previously reported algorithms. Furthermore, the spectral accuracy and spectral recovery performance can be substantially improved by interpolating the precalibration data using the new algorithm. As a result, with $10\times$ interpolation, the QD spectrometer here achieves an extremely high spectral accuracy as low as 0.1 nm and a spectral resolution of 2 nm in the 400 to 800 nm range, which represents the highest spectral accuracy among QD spectrometers.

2 Results and Discussion

Figure 1 shows the fabrication process of the QD spectrometer. Overall, we selected four different components of QDs for the spectral encoding, including CdS, CdS_xSe_{1-x}, CdSe, and CdTe QDs. Based on these components, a uniform and complete coverage of the absorption peaks of the synthesized QDs in the range of 400 to 800 nm was achieved by controlling the growth time of the QDs after the hot injection. Subsequently, the QD filter array was fabricated using electrohydrodynamic jet printing on a quartz substrate, which allowed for the small size and uniform distribution of individual QDs in the arrays. Finally, the substrate with the filter array was mounted on top of the CMOS image sensor using a UV-curable adhesive. A robust reconstruction algorithm with supreme noise tolerance performance was proposed to accomplish the spectral reconstruction, which integrates Tikhonov regularization and TV regularization techniques, along with the introduction of the alternating direction method of multipliers (ADMM).

The CdS, CdSe, CdS_xSe_{1-x}, and CdTe QDs were synthesized in a seeded growth manner. For a given composition, small QDs were formed by hot-injection synthesis with a highly excessive Cd precursor; then the chalcogenide precursor was added dropwise to promote continuous growth of the QDs. The synthetic parameters were carefully controlled to maintain the very distinguishable exciton peaks during the whole growth process. Aliquots were withdrawn from the growth solution at different intervals to obtain a series of QDs with increasing sizes. Through the control of composition and size, we managed to produce QDs with absorption peaks covering the visible light range. Figure 2(a) shows some solution samples of the QDs. A series of typical absorption spectra are shown in Fig. 2(b), and all the absorption spectra of the QDs used in this work are shown in Fig. S1 in the Supplemental Material. Typical transmission electron microscope images of the four types of QDs are shown in Fig. S2 in the Supplemental Material. In order to avoid interference from QD photoluminescence (PL), a fluorescence quencher was introduced to quench the PL,[28] as shown in Fig. S3 in the Supplemental Material. It is worth noting that the seeded growth is an advisable strategy to synthesize a series of QDs with different sizes. Figure 2(c) shows the absorption peak wavelength as a function of sampling time for the four types of QDs (two starting sizes were used for CdSe QDs), demonstrating the convenience of material preparation for QD spectrometers.

To prepare QD microfilters, the QDs were mixed with organic polymers, and the electrohydrodynamic jet printing technique was used to print them on a quartz substrate. Subsequently, a QD filter array was obtained through solvent evaporation and heat treatment. The native ligands on the QD surface are oleate, making them soluble only in nonpolar solvents, such as n-hexane and n-octane, whereas typical polymers have low solubility in these nonpolar solvents. To address this issue, we replaced the oleate ligand with a thiol ligand, 6-mercaptohexanol (MCH).[29,30] Simultaneously, it was observed that there was a slight change in the absorption peak of the QDs after ligand exchange, as shown in Fig. 3(a). This demonstrates that by controlling the duration and ligand concentration in the ligand exchange process, we can further fine-tune the absorption peak distribution of the QDs, achieving a more uniform spectral encoding effect. In addition to treatment on QDs, the selection of polymers must also meet certain criteria. First, the polymer itself must be highly transparent to visible light to avoid unnecessary light flux loss. Furthermore, the polymer must have good solubility in the chosen solvent and good compatibility with QDs. This helps ensure the uniformity of the printed QD filter,

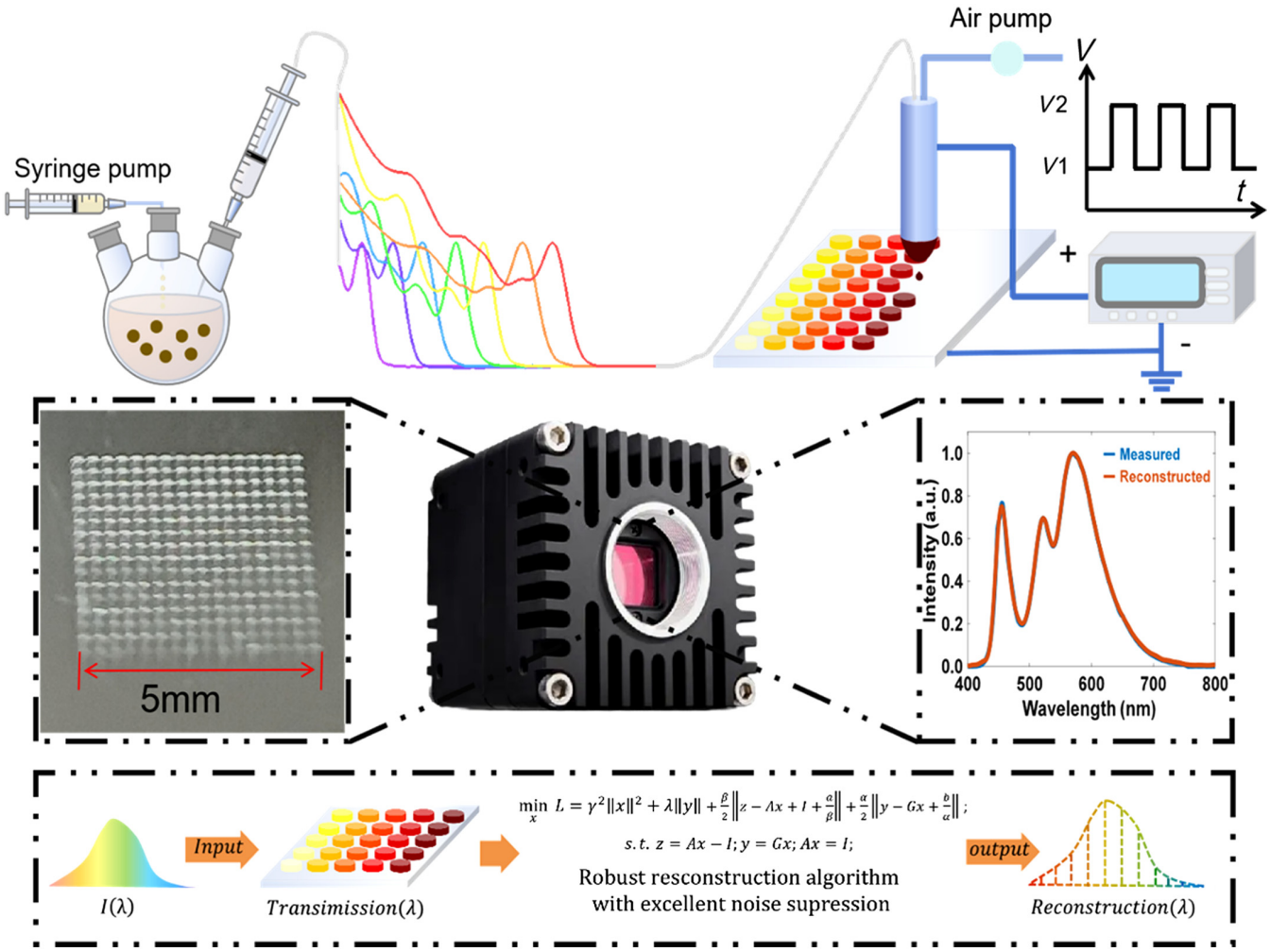

Fig. 1 The strategy for fabricating the QD spectrometer. The absorption spectra of the QDs are tuned via their size and composition, and the QD filter array is fabricated by the electrohydrodynamic jet printing technique. The substrate with the QD filter array is assembled on top of a CMOS image sensor to fabricate the spectrometer. A new reconstruction algorithm is proposed to enhance the noise tolerance performance.

avoiding light intensity loss caused by the optical structure on the filter surface, thus eliminating influence on the final encoding effect.[31] After comparative analysis (Fig. S4 in the Supplemental Material), we chose a binary solvent system of dimethyl sulfoxide (DMSO) and butanol and used polyvinylpyrrolidone (PVP) as the polymer. Figure 3(b) shows the printed QD filter array, demonstrating the orderly distribution of the microfilters. We tested the height of the printed microfilters using a profilometer, as displayed in Fig. 3(c), confirming that these QD filters have a smooth surface morphology. The QD filter array used for the spectrometer consists of a total of 256 microfilters, with an average size of 250 μm, a space of 70 μm, and an array size of only 0.50 cm × 0.50 cm. This array size is the smallest one reported to date. After obtaining the QD filter array, we assembled it on top of a CMOS image sensor. Then, precalibration was performed by collecting the data at every 1 nm in the range of 400 to 800 nm, producing transmission spectra of every microfilter; Fig. 3(d) shows some of the transmission spectra.

The CMOS camera was equipped with the QD filter array, which, combined with a spectral reconstruction algorithm, can work as a spectrometer.[32] The incident light passes through the spatially distributed 256 QD microfilters and is modified to varying degrees at different wavelengths, and the resulting signals are captured by the camera. The problem of reconstructing the input spectrum can be described as

$$\begin{aligned} &\min_x \|Ax - I\|_{L_2} \\ &s.t.\ \ Ax = I, \end{aligned} \tag{1}$$

where A is acquired before using the spectrometer, I is the signal collected by the camera, and x is to be reconstructed and further used to get the input spectral. The derivation of the mathematical model is described in detail in the Supplemental Material. A number of algorithms have been used for this problem.[33,34] These algorithms can be categorized into two types: general iterative algorithms and deep-learning algorithms. Compared to

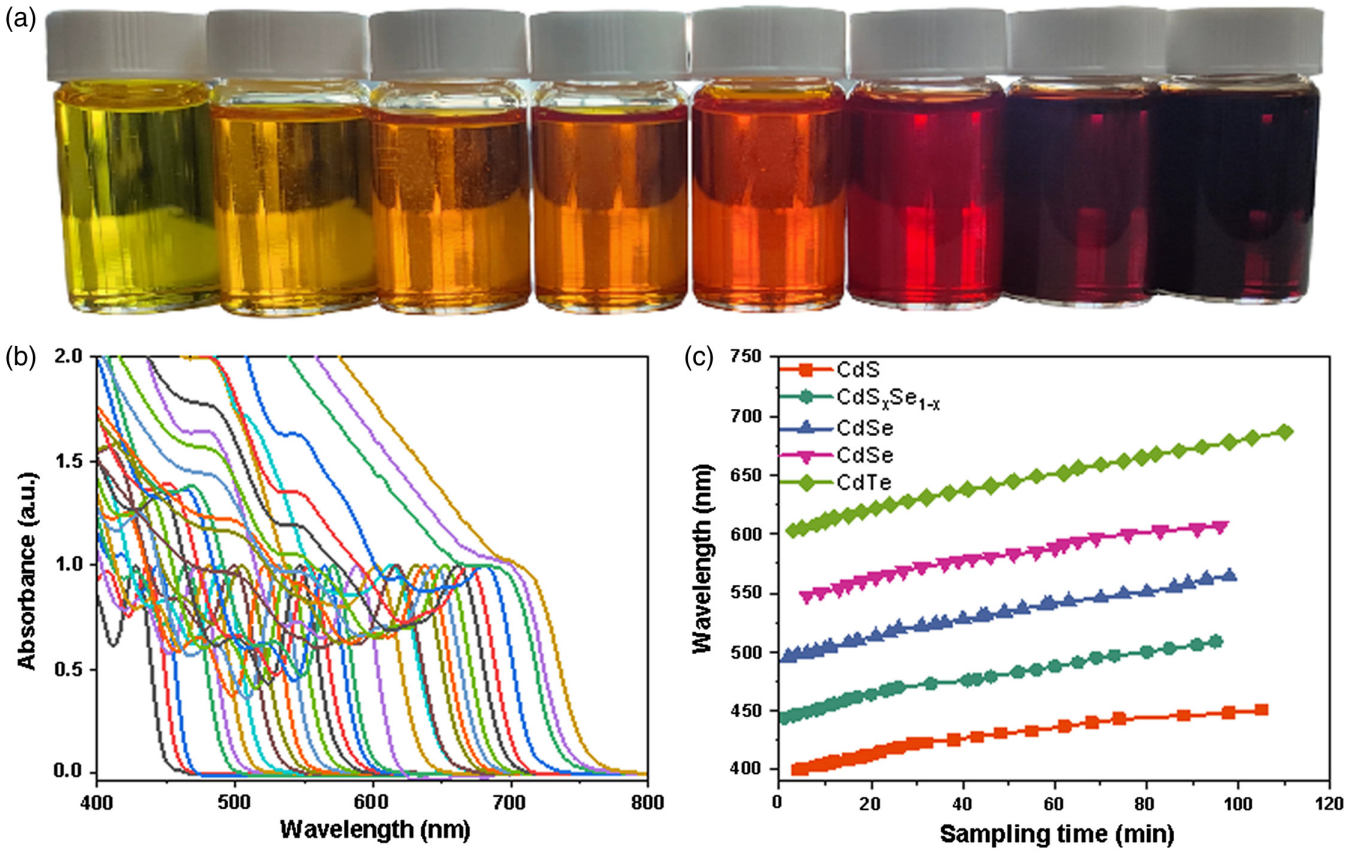

Fig. 2 (a) A picture of some typical QD solutions. (b) Absorption spectra of selected QDs. (c) Plots of QD absorption peak as a function of growth time in the seeded growth process for the QDs with different compositions.

general iterative algorithms, deep-learning algorithms usually use an end-to-end structure that requires a large amount of real data for data training.[35–39] And, although the model obtained after one training can directly solve the equation, on large-scale manufacturing, it is obviously not cost-effective to train each spectrometer individually. This places a high demand on the consistency of the fabricated encoding arrays. The general iterative strategy is usually based on the theory of compressive sensing theory, which may be slightly inferior to deep learning in terms of reconstruction effect, but relies on many fewer computational resources and faces less practical difficulty. Therefore, in this work, we adopted the general iterative strategy.

We initially used the Tikhonov regularization technique, commonly known as Ridge regression, for spectral reconstruction, as employed in the majority of previous works.[14,18,40] Due to the inclusion of the regularization term, the influence of noise on the reconstruction results during the iterative process is effectively suppressed. Using this algorithm, we reconstructed several monochromatic lights and compared the results with those collected by a commercial spectrometer, as shown in Fig. 4(a). For the monochromatic light, Ridge regression demonstrated good reconstruction performance. However, when this algorithm was applied to reconstruct broad spectra, the reconstruction results were not satisfactory, as shown in Fig. 4(b).

To improve the broad spectrum reconstruction performance of the algorithm, we considered the TV regularization technique commonly used in the field of image processing.[41] The essence of TV regularization is to impose constraints based on the continuity of data, typically expressed as the first-order derivative of the data in mathematical terms. This allows for a more suitable application for spectra with complex features. We named this model Ridge + TV and introduced the AdaDelta iterative strategy for parameter control, with detailed calculation procedures available in the Supplemental Material. As shown in Fig. S5 in the Supplemental Material, the introduction of the TV regularization term significantly improved the spectral reconstruction performance of the algorithm for the white LED spectrum.

To further improve the algorithm's noise tolerance, we believed that the role of the regularization term needed to be better utilized. The ADMM,[42] evolved from the Douglas–Rachford splitting method and Rockafellar's method of multipliers, figures out problems by alternately optimizing primal and dual variables, and updates the dual variables at each step using the method of Lagrange multipliers. This process effectively decomposes complex optimization problems into several subproblems for controlled resolution. Therefore, the ADMM was introduced to further enhance control over the regularization term. Moreover, the multistep iteration effect brought about by the method of ADMM allows us to more intuitively observe the impact of parameter changes during the iteration process of spectral reconstruction. We named this algorithm TKVA (algorithm with Tikhonov and TV regularization, and ADMM), and the mathematical model for the reconstruction problem becomes

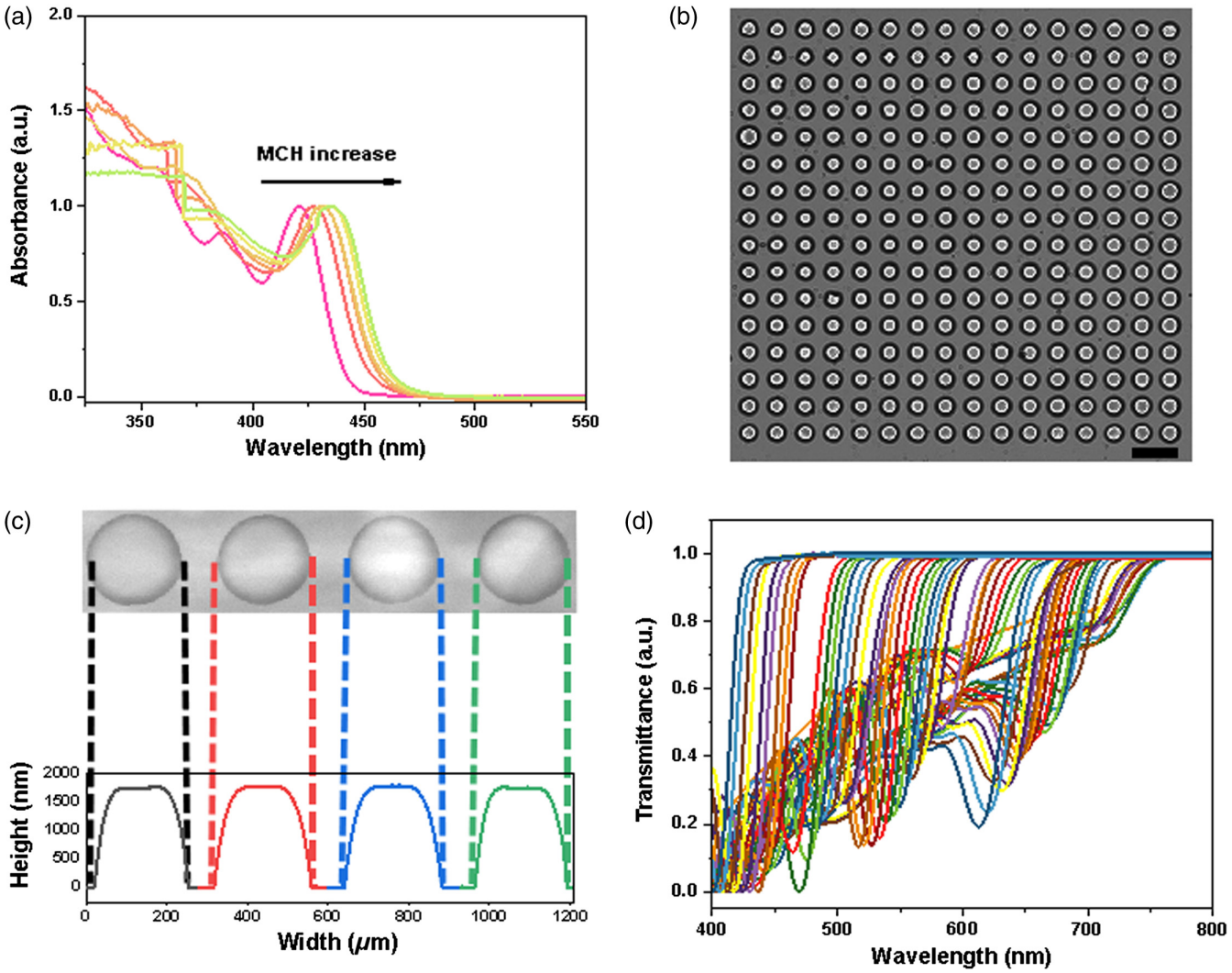

Fig. 3 (a) Redshift of the absorption peak of QDs with the increase of the MCH ligand. (b) A picture of the QD filter array, in which the scale bar is 0.50 mm. (c) Uniformity and surface profile of the filter units. (d) Transmittance spectra of some filter units.

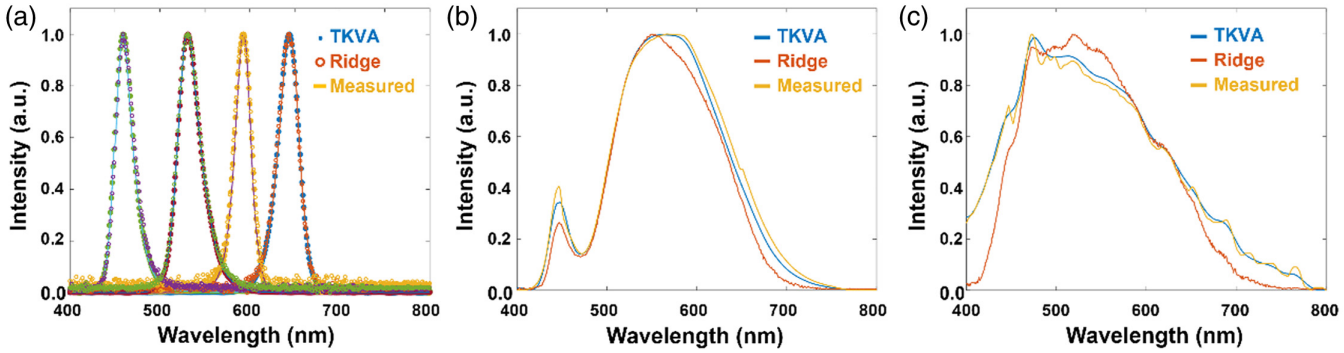

Fig. 4 Spectral reconstruction results of the TKVA algorithm for (a) monochromatic light, (b) a white LED spectrum, and (c) the xenon lamp spectrum. For comparison, the results of the Ridge algorithm are presented.

$$\min_x L = \gamma^2\|x\|^2 + \lambda\|y\| + \frac{\beta}{2}\|z - Ax + I + \frac{a}{\beta}\| + \frac{\alpha}{2}\|y - Gx + \frac{b}{\alpha}\|$$
$$s.t.\ z = Ax - I;\ y = Gx;\ Ax = I, \tag{2}$$

where γ is the Tikhonov regularization parameter, λ is the TV regularization parameter, α and β are the two augmented Lagrange penalty parameters of ADMM, and a and b are the parameter correction terms, respectively. G is the gradient computation matrix, which is matrix-multiplied with x to obtain TV parameter y.

First, the spectral reconstruction performance of the TKVA algorithm was evaluated. As shown in Figs. 4(a) and 4(b), the TKVA algorithm not only exhibits excellent spectral recovery for simple single peak spectra but also has supreme capability for the broad spectrum compared to the conventional Ridge regression algorithm. It is noteworthy that the TKVA algorithm shows significantly improved spectral recovery for complex broad spectra, such as the xenon lamp spectrum, as shown in Fig. 4(c).

Then, the noise tolerance of the TKVA algorithm was investigated. In fact, in the simulated spectral reconstruction process, the Ridge regression technique also demonstrated excellent reconstruction performance for broad spectra. However, this performance could not be retained in the actual measurement process, evidently due to the influence of noise during the practical detection process. The sources of noise could stem from the measurement process or from measurement errors during the precalibration process. We simulated the influence of noise by adding the noise to the incident spectrum and performed the reconstruction accordingly. By manually adding noise and comparing the simulated reconstruction results with the actual reconstruction results, it was estimated that the SNR in the actual measurement process was ~10 dB. However, in certain situations, the SNR could decrease to 0 dB or even lower due to tremors, drastic environmental changes, etc.

The noise tolerance performance of the TKVA algorithm was evaluated by introducing varying levels of noise. As shown in Fig. 5(a), at an SNR of 10 dB, the TKVA, the Ridge+TV, and the commonly used Ridge regression and Lasso regression demonstrate good reconstruction results. However, as the SNR gradually decreases, except for TKVA, overfitting becomes increasingly prominent in other algorithms [Fig. 5(b)]. When the SNR drops to −3 dB, as shown in Fig. 5(c), only the TKVA is still able to accurately reconstruct the original spectral features. In addition, the TKVA algorithm was also compared to the ALM algorithm[26] that was previously proposed to suppress the noise influence. As a result, the TKVA still shows much better noise tolerance performance than the ALM algorithm, as shown in Fig. S6 in the Supplemental Material.

Spectral accuracy is a key figure of merit for spectrometers, and this performance of the QD spectrometer based on TKVA algorithm was evaluated. The computational spectrometer has to be precalibrated before operation, in which we scanned the monochromatic light with an interval of 1 nm. Theoretically, a smaller interval is beneficial for attaining a higher spectral accuracy, thus the 1 nm step might impose a constraint on the maximum accuracy. To overcome this limitation and considering the continuity of spectral distribution, we performed spline interpolation on the results obtained from the precalibration process. We conducted 1×, 2×, 5×, 10×, and 20× interpolations and reconstructed a simulated monochromatic light with a minimum full width at a half-maximum of 0.8 nm. The reconstruction results for different interpolation factors are shown in Figs. 6(a) and 6(b) using the TKVA and the Ridge algorithms, respectively. As the interpolation factor increases, the TKVA algorithm shows better reconstruction performance

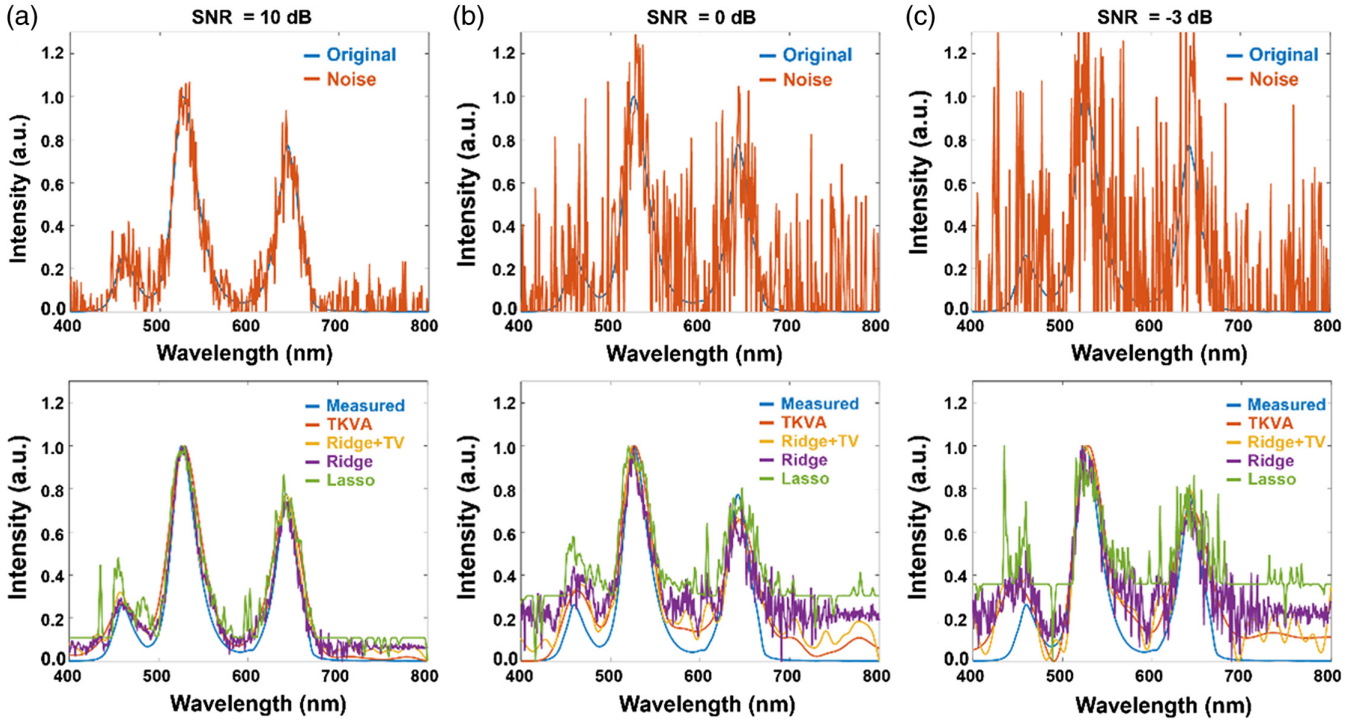

Fig. 5 Spectral reconstruction results of different algorithms at noise levels of (a) 10 dB, (b) 0 dB, and (c) −3 dB.

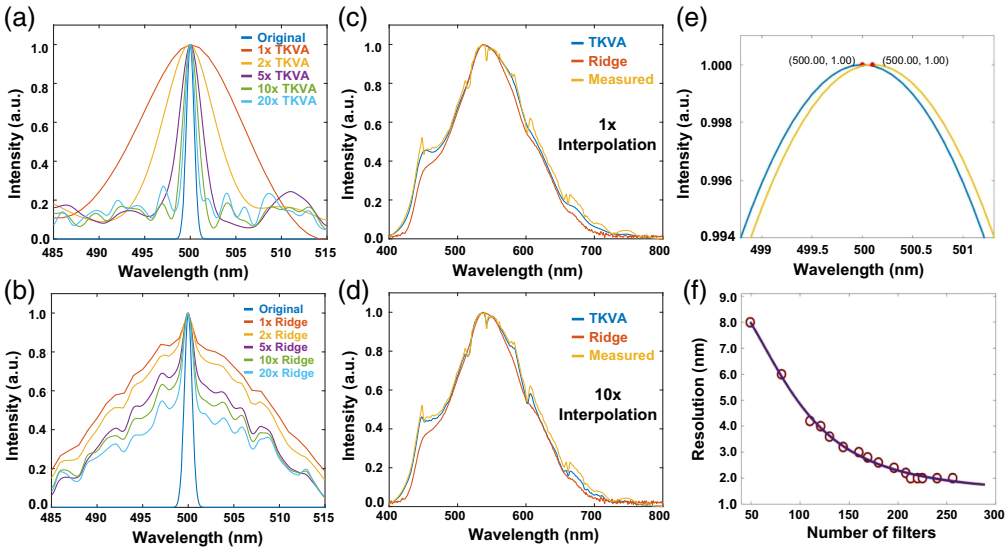

Fig. 6 Spectral reconstruction results of the (a) TKVA and (b) Ridge algorithms at different interpolation factors. Reconstruction results of room light (c) without and (d) with 10× interpolation using the TKVA and Ridge algorithms. (e) Reconstruction results of two monochromatic lights with peaks 0.1 nm apart. (f) Spectral resolution as a function of the number of QD filters.

for the narrow monochromatic light. Although data oscillation appears in the flat data regions at higher interpolation factors due to overfitting, it has little impact on distinguishing the peak [Fig. 6(a)]. In contrast, the improvement of the Ridge algorithm is substantially limited [Fig. 6(b)]. The interpolation effect of the ALM algorithm, which shows inferior reconstruction performance than that of the TKVA algorithm at the same level of interpolation, was also studied (Fig. S7 in the Supplemental Material). These results indicate the unique advantage of the TKVA algorithm on the enhancement of spectral accuracy. In practice, we also used data scanned every 3 nm for 15× interpolation for reconstruction and found that the spectral reconstruction performance was not significantly affected (Fig. S8 in the Supplemental Material). Therefore, the newly proposed TKVA algorithm not only offers a convenient and effective way to improve the spectral accuracy but also provides a route to reduce the workload of the precalibration process through interpolation.

To evaluate the spectral reconstruction performance with the help of interpolation, we reconstructed a complex and broad spectrum (room light) without interpolation and with 10× interpolation, as shown in Figs. 6(c) and 6(d), respectively. After interpolation, the recovery performance of the TKVA algorithm is significantly improved, which not only exhibits more accurate overall reconstruction but also captures small peaks in the spectrum. In contrast, the Ridge algorithm shows little improvement via interpolation and exhibits much poorer reconstruction performance. With a significant improvement in noise tolerance and spectral recovery by interpolation, the TKVA algorithm shows a relatively modest increase in usage of computing resources; for example, under 10-fold interpolation, the TKVA algorithm requires 0.025 s to reconstruct a single-peak spectral, while the Ridge + TV algorithm needs 0.008 s.

Finally, we investigated the spectral accuracy of the TKVA-based QD spectrometer with actual monochromatic light input; the results are shown in Fig. 6(e). After calculation, the spectral accuracy of the spectrometer in the 400 to 800 nm range reaches as low as 0.1 nm, representing the highest level for QD spectrometers.[26,28,29,43,44] In addition, we investigated the influence of the number of QD filters on spectral reconstruction, as shown in Fig. 6(f). As the number increases, the average spectral resolution increases accordingly, which reaches a value of 2 nm, as shown in Fig. S9 in the Supplemental Material. After the number reached 196, further increasing the number of the filter results in a slight improvement in resolution, indicating a limited number of filters are adequate to achieve a high spectral resolution.

3 Conclusions

In summary, we demonstrate a high spectral accuracy QD spectrometer with excellent noise tolerance by developing a new reconstruction algorithm. Seeded growth is adopted to produce a series of QDs with increasing size, and the absorption peak of all the QDs used is finely tuned by the combination of size and composition in the range of 400 to 800 nm. The electrohydrodynamic jet printing technique is applied to fabricate the QD filter array with a total number of 256, a filter size of 250 μm, and a space of 70 μm. The filter array on a quartz substrate is assembled on top of a CMOS image sensor to form the spectrometer. In order to enhance the noise tolerance performance, a new algorithm, TKVA, was proposed, which integrates Tikhonov regularization and TV regularization techniques, along with the introduction of the ADMM. The TKVA algorithm shows excellent noise tolerance demonstrated by good spectral recovery even at a low SNR of −3 dB, outperforming previously reported algorithms. In addition to noise tolerance, the TKVA algorithm offers a unique advantage compared to other algorithms; that is, the spectral accuracy can be improved by interpolation of the data obtained in the precalibration process. In the meantime, the spectral reconstruction performance is also significantly improved especially for complex and broad

spectra, which is not observed for other algorithms. Through interpolation, the TKVA can reduce the workload of the precalibration process while maintaining a high spectral recovery performance. Based on the TKVA algorithm, the QD spectrometer shows a spectral accuracy as low as 0.1 nm in the range of 400 to 800 nm, representing the highest level among QD spectrometers. The supreme TKVA algorithm might find broad applications in different types of computational spectrometers.

4 Appendix: Materials and Methods

4.1 Chemicals and Reagents

Cadmium oxide (CdO, 99.99%), oleic acid (OA, AR), sulfur powder (S, 99.9%), selenium powder (Se, 99.99%), 1-octadecene (ODE, 90%), methanol (MeOH, 99.5%), acetone (CH_3COCH_3, 99.5%), dimethyl sulfoxide (DMSO, 95%), and thiol ligand (MCH, 98%) were purchased from Aladdin. Trioctylphosphine (TOP, 90%), tellurium granules (Te, 99.99%), tributylphosphine (TBP, 98%), polyvinylpyrrolidone (PVP, GR), and cellulose acetate (CA) were bought from Macklin.

4.2 Synthesis and Sampling of QDs

Initially, a mixture of CdO (6.4 g, 0.05 mol), OA (50 g, 0.177 mol), and ODE (150 g, 0.600 mol) was heated under an inert gas protection to 250°C, resulting in the precursor solution of Cd. Subsequently, the anion source was rapidly injected into the reaction system. After maintaining for a certain duration, the appropriately diluted anion precursor solution was slowly injected into the reaction flask using a syringe pump to promote the continuous growth of QDs. At specific time intervals during the QD growth process, 5 mL samples of the reaction solution were extracted until the complete collection of all QD materials was obtained. The starting size of the QDs was controlled by regulating the temperature of thermal injection and the amount of precursor solution injected. Once all the QD materials were collected, they were thoroughly washed and purified multiple times using methanol and acetone.

4.3 Preparation and Printing of QD Inks

The purified QDs were dissolved in 10 mL of octane, and a small amount of MCH solution (20 to 100 μL) was added. After oscillation and centrifugation, the QDs with complete ligand exchange were obtained. These QDs were dissolved in a mixed solvent of DMSO and butanol. The concentration of each type of QDs was adjusted to achieve similar absorbance at 400 nm for all QDs. This step ensured that when all QDs were printed on a quartz substrate, their overall transmittance remained at a similar value. After the preparation of all QD inks, they were printed on quartz slides using the electrohydrodynamic jet printing technique, and the solvent was evaporated using a hot plate. The printing equipment used is displayed in Fig. S10 in the Supplemental Material.

4.4 Precalibration of the Spectrometer and Spectral Reconstruction

Before operating the spectrometer, the $R_i(\lambda)$ needs to be collected first. Thus, in the precalibration process, spatially uniform monochromatic light was input into a CMOS camera. The wavelength was scanned from 400 to 800 nm, and a picture was taken at each step (1 nm). Then, the substrate with a QD filter array was assembled on top of the CMOS image sensor, and the wavelength scan and taking a picture were repeated. $R_i(\lambda)$ was calculated based on the signals of the pixel under a filter unit with and without the filter array. Then, the spectrometer was ready for measurement and spectral reconstruction.

Disclosures

The authors declare no conflicts of interest.

Code and Data Availability

The data sets are available from the corresponding author upon request.

Acknowledgments

This work was supported by the National Key Research and Development Program of China (Grant No. 2021YFA0715502), the National Natural Science Foundation of China (Grant Nos. 61974052, U22A2083, 62204091, 62374068, and 62304085), the Scientific Research Project of Wenzhou (Grant No. G2023025), the Innovation Project of Optics Valley Laboratory (Grant No. OVL2023ZD002), the Exploration Project of Natural Science Foundation of Zhejiang Province (Grant No. LY23F040005), and the Fund from Science, Technology, and Innovation Commission of Shenzhen Municipality (Grant Nos. GJHZ20210705142540010 and GJHZ20220913143403007). The authors thank the Testing Center of Huazhong University of Science and Technology.

References

1. Z. Yin et al., "Quantum-dot light-chip micro-spectrometer," *Opt. Lett.* **48**, 3371 (2023).
2. M. Pawlyta, J. N. Rouzaud, and S. Duber, "Raman microspectroscopy characterization of carbon blacks: spectral analysis and structural information," *Carbon* **84**, 479 (2015).
3. N. Ozbek and S. Akman, "Determination of fluorine in Turkish wines by molecular absorbance of CaF using a high resolution continuum source atomic absorption spectrometer," *LWT Food Sci. Technol.* **61**, 112 (2015).
4. J. Zou et al., "Novel high-resolution and large-bandwidth microspectrometer using multi-input counter-propagating arrayed waveguide grating and dual-wavelength grating coupler on silicon on insulator," *Laser Photonics Rev.* **17**, 2200355 (2023).
5. L. Gao et al., "Computational spectrometers enabled by nanophotonics and deep learning," *Nanophotonics* **11**, 2507 (2022).
6. C.-C. Chang and H.-N. Lee, "On the estimation of target spectrum for filter-array based spectrometers," *Opt. Express* **16**, 1056 (2008).
7. J. Oliver, W.-B. Lee, and H.-N. Lee "Filters with random transmittance for improving resolution in filter-array-based spectrometers," *Opt. Express* **21**, 3969 (2013).
8. E. Huang, Q. Ma, and Z. Liu, "Etalon array reconstructive spectrometry," *Sci. Rep.* **7**, 40693 (2017).
9. Y. Horie et al., "Visible wavelength color filters using dielectric subwavelength gratings for backside-illuminated CMOS image sensor technologies," *Nano Lett.* **17**, 3159 (2017).
10. K. M. Bryan et al., "Inexpensive photonic crystal spectrometer for colorimetric sensing applications," *Opt. Express* **21**, 4411 (2013).
11. J. Zhang et al., "Cascaded nanobeam spectrometer with high resolution and scalability," *Optica* **9**, 517 (2022).
12. C. Yao et al., "Broadband picometer-scale resolution on-chip spectrometer with reconfigurable photonics," *Light Sci. Appl.* **12**, 156 (2023).

13. A. Li and Y. Fainman, "On-chip spectrometers using stratified waveguide filters," *Nat. Commun.* **12**, 2704 (2021).
14. Z. Yang et al., "Single-nanowire spectrometers," *Science* **365**, 1017 (2019).
15. J. J. Cadusch et al., "Compact, lightweight, and filter-free: an all-Si microspectrometer chip for visible light spectroscopy," *ACS Photonics* **9**, 474 (2022).
16. Y. Chang et al., "Development of triboelectric-enabled tunable Fabry-Pérot photonic-crystal-slab filter towards wearable mid-infrared computational spectrometer," *Nano Energy* **89**, 106446 (2021).
17. Y. August and A. Stern, "Compressive sensing spectrometry based on liquid crystal devices," *Opt. Lett.* **38**, 4996 (2013).
18. S. Yuan et al., "A wavelength-scale black phosphorus spectrometer," *Nat. Photonics* **15**, 601 (2021).
19. H. H. Yoon et al., "Miniaturized spectrometers with a tunable van der Waals junction," *Science* **378**, 296 (2022).
20. A. L. Rogach et al., "Infrared-emitting colloidal nanocrystals: synthesis, assembly, spectroscopy, and applications," *Small* **3**, 536 (2007).
21. E. H. Sargent, "Infrared quantum dots," *Adv. Mater.* **17**, 515 (2005).
22. W. W. Yu et al., "Experimental determination of the extinction coefficient of CdTe, CdSe, and CdS nanocrystals," *Chem. Mater.* **15**, 2854 (2003).
23. B. Cerjan and N. J. Halas, "Toward a nanophotonic nose: a compressive sensing-enhanced, optoelectronic mid-infrared spectrometer," *ACS Photonics* **6**, 79 (2019).
24. C. Kim et al., "Mass production-enabled computational spectrometers based on multilayer thin films," *Sci. Rep.* **12**, 4053 (2022).
25. K. Dong et al., "Single-pixel reconstructive mid-infrared microspectrometer," *Opt. Express* **31**, 14367 (2023).
26. X. Zhu et al., "Broadband perovskite quantum dot spectrometer beyond human visual resolution," *Light Sci. Appl.* **9**, 73 (2020).
27. J. Zhang, X. Zhu, and J. Bao, "Denoising autoencoder aided spectrum reconstruction for colloidal quantum dot spectrometers," *IEEE Sens. J.* **21**, 6450 (2021).
28. J. Bao and M. G. Bawendi, "A colloidal quantum dot spectrometer," *Nature* **523**, 67 (2015).
29. H. Li et al., "A near-infrared miniature quantum dot spectrometer," *Adv. Opt. Mater.* **9**, 2100376 (2021).
30. D. Grodzińska et al., "Two-fold emission from the S-shell of PbSe/CdSe core/shell quantum dots," *Small* **7**, 3493 (2011).
31. V. Wood et al., "Inkjet-printed quantum dot–polymer composites for full-color AC-driven displays," *Adv. Mater.* **21**, 2151 (2009).
32. S. Yuan et al., "Geometric deep optical sensing," *Science* **379**, eade1220 (2023).
33. J. Meng, J. J. Cadusch, and K. B. Crozier, "Detector-only spectrometer based on structurally colored silicon nanowires and a reconstruction algorithm," *Nano Lett.* **20**, 320 (2020).
34. D. Tua et al., "Imaging-based intelligent spectrometer on a plasmonic rainbow chip," *Nat. Commun.* **14**, 1902 (2023).
35. J. Wen et al., "Deep learning-based miniaturized all-dielectric ultracompact film spectrometer," *ACS Photonics* **10**, 225 (2023).
36. J. Zhang, X. Zhu, and J. Bao, "Solver-informed neural networks for spectrum reconstruction of colloidal quantum dot spectrometers," *Opt. Express* **28**, 33656 (2020).
37. W. Zhang et al., "Deeply learned broadband encoding stochastic hyperspectral imaging," *Light Sci. Appl.* **10**, 108 (2021).
38. Q. Zheng et al., "On-chip near-infrared spectral sensing with minimal plasmon-modulated channels," *Laser Photonics Rev.* **17**, 2300475 (2023).
39. J. Wang et al., "Perovskite single-detector visible-light spectrometer," *Opt. Lett.* **48**, 399 (2023).
40. G. Wu et al., "Miniaturized computational spectrometer," *IEEE Nanotechnol. Mag.* **17**, 36 (2023).
41. A. Marquina and S. J. Osher, "Image super-resolution by TV-regularization and Bregman iteration," *J. Sci. Comput.* **37**, 367 (2008).
42. Y. Wang, W. Yin, and J. Zeng, "Global convergence of ADMM in nonconvex nonsmooth optimization," *J. Sci. Comput.* **78**, 29 (2019).
43. C. Venettacci et al., "Algorithm-based spectrometer exploiting colloidal PbS quantum dots," *Photonics Nanostruct. Fundam. Appl.* **43**, 100861 (2021).
44. A. De Iacovo et al., "Narrowband colloidal quantum dot photodetectors for wavelength measurement applications," *Nanoscale* **12**, 10044 (2020).
45. D. Marić and J. P. Burrows, "Application of a Gaussian distribution function to describe molecular UV−visible absorption continua. 1. Theory," *J. Phys. Chem.* **100**, 8645 (1996).
46. J. Verrelst et al., "Spectral band selection for vegetation properties retrieval using Gaussian processes regression," *Int. J. Appl. Earth Obs. Geoinf.* **52**, 554 (2016).
47. E. J. Candes, J. Romberg, and T. Tao, "Robust uncertainty principles: exact signal reconstruction from highly incomplete frequency information," *IEEE Trans. Inf. Theory* **52**, 489 (2006).
48. D. L. Donoho, "Compressed sensing," *IEEE Trans. Inf. Theory* **52**, 1289 (2006).

Biographies of the authors are not available.